This article has been accepted for inclusion in a future issue of this journal. Content is final as presented, with the exception of pagination.



# So-EAGlove: VR Haptic Glove Rendering Softness Sensation With Force-Tunable Electrostatic Adhesive Brakes

Quan Xiong, Xuanquan Liang, Daiyue Wei, Huacen Wang, Renjie Zhu, *Graduate Student Member, IEEE*, Ting Wang, Jianjun Mao, and Hongqiang Wang, *Member, IEEE*

***Abstract*—Haptic gloves allow the players to feel the virtual world more realistically by providing force feedback. At present, haptic gloves are mainly driven by conventional motors, and for them, being lightweight, low cost, low in power consumption, and intrinsically safe to operators are challenging. Here, we designed a haptic glove (So-EAGlove) integrating a flexible electrostatic adhesive brake to resist human fingers with a tunable braking force and render a softness sensation. This glove weighs only 51 g, but is capable of simulating objects in a large range of Young's modulus from 540 Pa to 5.4 MPa. The electrostatic adhesive brake costs only approximately 2.43 mW during operation, i.e., more than three days powered by a small button battery. We built a feedforward control model and evaluated its performance. Experimental results show that this glove can generate an accurate force to follow the force-displacement profile of the corresponding real objects. The error is less than 7%, barely noticeable by the subjects. The subjective tests also demonstrate that little statistical difference exists between the real objects and the virtual objects for the subjects.**

***Index Terms*—Electrostatic adhesion (EA), force feedback, haptic glove, softness sensation, variable stiffness, virtual reality (VR).**

Manuscript received December 7, 2021; revised April 13, 2022; accepted April 25, 2022. This work was supported in part by the National Natural Science Foundation for Young Scientists of China under Grant 51905256, in part by the Natural Science Foundation of Guangdong Province of China under Grant 2020A1515010955, in part by the Science, Technology and Innovation Commission of Shenzhen Municipality under Grant ZDSYS20200811143601004, in part by the Natural Science Foundation of Liaoning Province of China (State Key Laboratory of Robotics joint funding, under Grant 2021-KF-22-11), and in part by Southern Marine Science and Engineering Guangdong Laboratory (Guangzhou)?under Grant K19313901. This paper was recommended for publication by Associate Editor H. Zhao and Editor E. Yoshida upon evaluation of the reviewers' comments. (*Corresponding author: Hongqiang Wang.*)

Quan Xiong, Huacen Wang, Renjie Zhu, Ting Wang, and Jianjun Mao are with the Shenzhen Key Laboratory of Biomimetic Robotics and Intelligent Systems, Department of Mechanical and Energy Engineering, Southern University of Science and Technology, Shenzhen 518055, China (e-mail: e0788090@u.nus.edu; 12132296@mail.sustech.edu.cn; zhurj@mail.sustech.edu.cn; twang264-c@my.cityu.edu.hk; 11849009@mail.sustech.edu.cn).

Xuanquan Liang and Daiyue Wei are with the Guangdong Provincial Key Laboratory of Human-Augmentation and Rehabilitation Robotics in Universities, Southern University of Science and Technology, Shenzhen 518055, China (e-mail: 11930624@mail.sustech.edu.cn; weidy@mail.sustech.edu.cn).

Hongqiang Wang is with the Shenzhen Key Laboratory of Biomimetic Robotics and Intelligent Systems, Department of Mechanical and Energy Engineering and Guangdong Provincial Key Laboratory of Human-Augmentation and Rehabilitation Robotics in Universities, Southern University of Science and Technology, Shenzhen 518055, China, and also with the Southern Marine Science and Engineering Guangdong Laboratory (Guangzhou), Guangzhou 510000, China (e-mail: wanghq6@sustech.edu.cn).

This article has supplementary material provided by the authors and color versions of one or more figures available at https://doi.org/10.1109/TRO.2022.3172498.

Digital Object Identifier 10.1109/TRO.2022.3172498

## I. Introduction

VIRTUAL reality (VR) is an emerging technology that creates a simulated environment through artificial vision, sounds, haptics, and other sensation similar to the real world [1]. This technique has been attractive in both industry and academia in the last decades for vast applications such as entertainment, manufacturing, healthcare, education, and the emerging metaverse [2]–[4]. Currently, most VR devices only render visual feedback [5]. Actually, in daily life, tremendous information is achieved by haptics [6]. Therefore, recently researchers have dedicated themselves to developing VR haptic devices, particularly those mounted on hands [7].

Typically, haptic gloves generate force by braking devices based on various driving mechanisms, such as pneumatic/hydraulic pressure, electromagnetic motor, and magnetorheological fluid [8]–[10]. Pneumatic/hydraulic pressured muscles are soft and compact but noisy in pressure source and less accurate in force control. Using commercially available electromagnetic motors or magnetorheological fluid are popular approaches. Still, the large weight and size cause fatigue on the arm and hand and diminish the realism of the simulated environment.

This article integrates the emerging electrostatic adhesion (EA) brake into the VR haptic glove. An EA brake is typically composed of two conductive layers and a dielectric layer between the conductors [11]–[14]. Supplied with high voltage, unlike charges are induced in the two conductive layers respectively, generating a resistance force on the interfaces. Since the EA brake is mainly made from polymers and in thin-film form, the glove with EA is supposed to be compact, lightweight, compliant, economical, and low in energy consumption (several milliwatts [15]). The EA brake is intrinsically safe since it generates resistance force passively only when it is subject to an external force, while the active motors might hurt human beings once they malfunction. Previously, a conceptual haptic glove has developed based on EA [15], showing the exciting advantages of EA on haptic gloves, such as lightweight and compactness, by rendering the virtual rigid objects using the ON and OFF statuses of EA brakes. For more extensive applications,

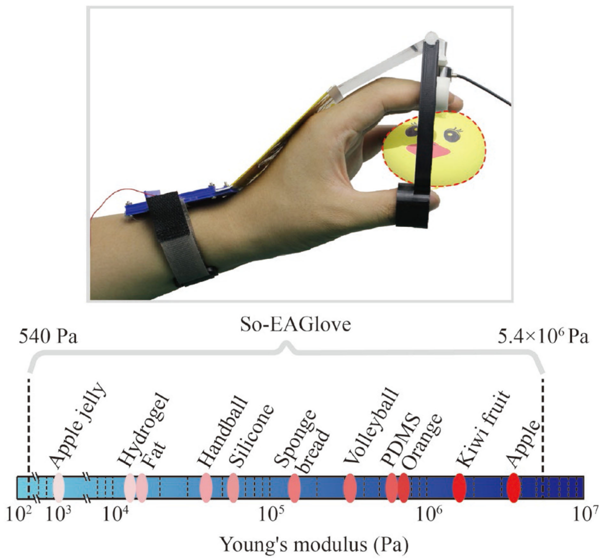


Fig. 1. So-EAGlove, a VR haptic glove integrating force-tunable EA brake while grasping a virtual balloon. The large range of objects and materials that can be simulated by So-EAGlove is shown below.

this promising technique needs to simulate a larger range of objects, e.g., soft items. However, there are many challenges to generating a softness sensation in the haptic glove system by EA brakes. For example, the model should be built to predict the force-displacement curvature of a virtual soft object. Next, to follow the aim force curvature accurately, the hardware and the control algorithm of EA brakes should be improved and evaluated.

The contributions of this article are as follows. Integrating an EA brake, we design and devise a lightweight, energy-efficient, compact haptic glove (So-EAGlove) capable of rendering a softness sensation. So-EAGlove (see Fig. 1) can simulate a large range of softness from 540 Pa (like jelly) to 5.4 MPa (similar to the apple). It weighs 51 g and consumes only 2.43 mW during operation (smaller than most previous haptic gloves [16]–[18]). We built the closed-loop control model for a haptic glove integrating an EA brake to eliminate disturbance on the adhesive force. The simulated force curvatures for springs, silicone blocks, and complex soft objects (e.g., a rubber duck and a piece of cake) possess minor errors that are barely perceivable (less than 7%). So-EAGlove also renders virtual soft objects (e.g., springs, silicone, and balloons) that cannot be distinguished by the participants from the real ones, according to the statistical analysis results of the subjective tests ($p>0.05$).

The structure of this article is as follows. The basic principle of the contact model of the finger, EA braking force, and the control model of EA braking force are explained in Section II. The manufacturing and assembly methods of the EA brake and the So-EAGlove are introduced in Section III in detail. In Section IV, the experimental results are exhibited and discussed. Lastly, we summarize this article and propose future work in Section V.

## II. Modeling

To understand the force variance of a virtual soft object, we build a contact force model. To generate controllable force, we establish a model for the EA brake. With the target force curvature predicted by the contact force model and the feedforward calculated from the EA brake model, we develop the closed-loop controller for the system. The detail is described as follows.

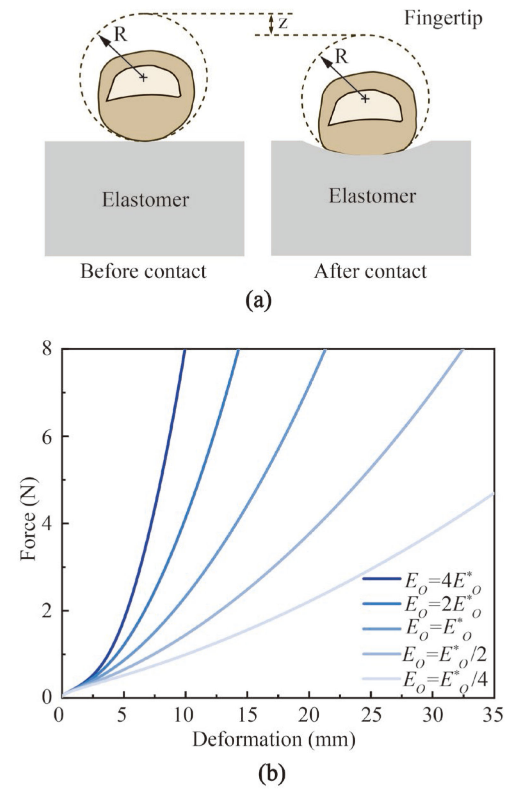


Fig. 2. Contact model. (a) Deformation process of elastomer pressed by a fingertip. (b) Influence of $E_o$ on contact model between fingertips and silicone. In the estimation, the value of $E^*{}_o$ is from silicone A and the parameters is from human fingertips. They were measured through preliminary experiments (mentioned in Section IV) at the pressing speed of 30 mm/min.

### A. Softness Sensation

One can assess the softness of an object by perceiving the applied force and corresponding deformation. The force on a spring or an ideal elastic object is proportional to the deformation

$$F = kx = \frac{ES}{L}x \tag{1}$$

where $k$ is the stiffness (if the object is a spring), $x$ is the displacement, $E$ is the equivalent Young's modulus if the object is an elastic item, $S$ is the contact area, and $L$ is the height of the simulated sample. This equation is just a simple model for an ideal elastomer by neglecting the nonlinear factors such as the internal damping of the elastomer and the finger elasticity. If considering these factors in the practical elastomer, the contact force $F$ can be calculated by

$$F = F_e + F_v \tag{2}$$

where $F_v$ is the internal damping force expressed by

$$F_v = c\dot{z}\sqrt{z} \tag{3}$$

where $c$ is a constant, and $z$ is the deformation [see Fig. 2(a)]. $F_e$ is the elastic force owing to deformation based on Hertzian

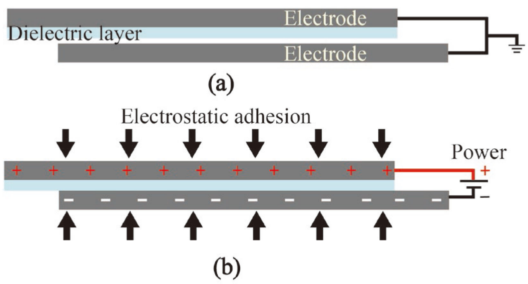


Fig. 3. Principle of EA. (a) Voltage is OFF. (b) Voltage is ON.

contact model

$$F_e = \frac{2E\sqrt{R}}{3} z^{\frac{3}{2}} \tag{4}$$

where *R* is the fingertip radius, and *E* is the equivalent Young's modulus calculated by

$$\frac{2}{E} = \frac{1 - {v_f}^2}{E_f} + \frac{1 - {v_o}^2}{E_o} \tag{5}$$

where $v_f$ and $v_o$ are the Poisson's ratios of the fingertip and the object, and $E_f$ and $E_o$ are Young's modulus of the fingertip and the object, respectively. In the case of large deformation [19], the elastic modulus $E_o$ and $E_f$ are functions of contact force $F$

$$E_f(F) = E_{f1}F + E_{f2} \tag{6}$$

$$E_o(F) = E_{o1}F + E_{o2} \tag{7}$$

where $E_{f1}$, $E_{f2}$, $E_{o1}$, and $E_{o2}$ are constant coefficients. In this contact model, we assume the nonlinear elastic materials are isotropic. Hence, if the parameters of materials are given, the model can reproduce the force-displacement curves. This model can be employed for a physical engine in the VR system to real-time calculate the tendency of the interacting force from a set of parameters.

According to the equations above, the pressing force (contact force) on an elastomer non-linearly increases with the deformation, as shown in Fig. 2(b). Larger elasticity makes both the force and the increasing ratio higher. To render an elastic perception, we should generate a force with such a tendency too. The above model assumes the soft object is a large compliant block. Complex objects composed of multiple components and materials can be roughly estimated by this model by simplifying the objects into an equivalent simple structure or be precisely predicted with modified models [20].

The magnitude of the force curvature rendered by the haptic device can have a little error since the skin perception has a certain tolerance, which is the just noticeable difference (JND), approximately 7% of the reference force [21].

### B. EA Braking Force

A typical EA brake is composed of two electrodes and a dielectric layer between them. When a voltage is applied to the two electrodes, unlike charges are induced, and friction is generated by the Coulomb force between the charges (see Fig. 3). The normal EA force between the electrodes can be simply calculated by the parallel-plate capacitance model

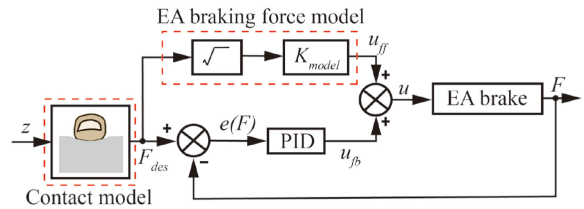


Fig. 4. Control diagram of EA braking force.

$$F_{\text{adhesive}} = \frac{\varepsilon_r \varepsilon_0 A U^2}{2d^2} \tag{8}$$

where *U* is the applied voltage, $\varepsilon_r$ is the dielectric constant of the insulation layer, $\varepsilon_0$ is the vacuum permittivity, *A* is the overlap area of the two electrodes, and $d$ is the thickness of the dielectric layer. EA force which is perpendicular to the films causes friction force (EA braking force) between the thin films

$$F_{\text{braking}} = \mu F_{\text{adhesive}} \tag{9}$$

where $\mu$ is the coefficient of friction. Ideally, we can control EA braking force by just tuning the voltage according to the above equations, but the error is large in practice since the above equations neglect other factors that are non-linear and time-variant, such as leakage current, accumulated charges, and mechanical deformation of the electrodes [22]–[24]. In this article, we decide to compensate for the discrepancy between the above ideal model and target force by a closed-loop control, which is explained in the next part.

### C. Closed-Loop Control With Feedforward

Although the mechanism of EA has been extensively studied, little literature explores the controllers [25], [26], particularly those with force feedback. It is more challenging to control the EA force of brakes that are made of flexible and deformable films than the EA devices with rigid or stiff electrodes [25], [26]. Here we introduce feedback control to improve the accuracy and response of the system (see Fig. 4) by adopting a proportional-integral-derivative (PID) controller for the closed-loop control. The target force-displacement curvature is generated by the contact model. However, based on our tests, only the PID controller is difficult to achieve both high accuracy and fast response simultaneously. Therefore, we introduce the feedforward into the controller, which is derived from the EA braking force model. The control voltage is expressed by

$$u = u_{fb} + u_{ff} \tag{10}$$

$$u_{fb} = K_p e + K_i \int e dt + K_d \dot{e} \tag{11}$$

$$u_{ff} = K_{\text{model}} \sqrt{F_{\text{des}}} \tag{12}$$

where $K_p$, $K_i$, and $K_d$ are the closed-loop control parameters, $u_{fb}$ and $u_{ff}$ are the feedback voltage and the feedforward voltage, respectively, and $F_{\text{des}}$ is the target force, $K_{\text{model}}$ is the EA braking force model parameter depending on the dimensions and material property of the EA brake, achieved

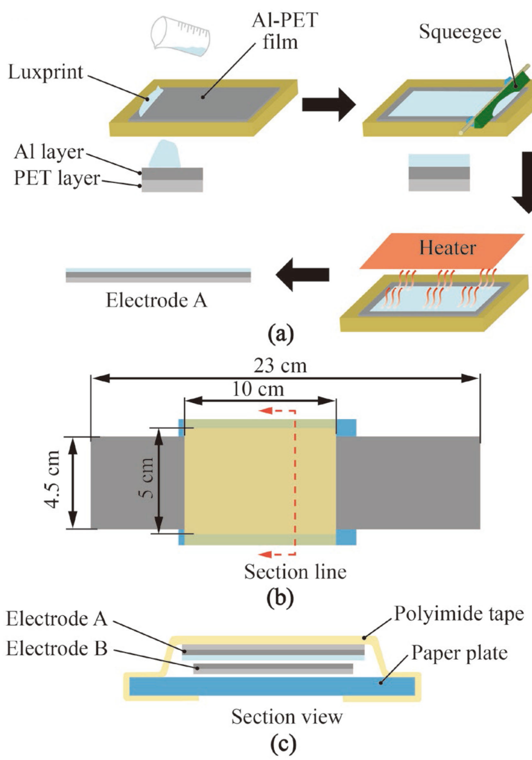


Fig. 5. Fabrication of the EA brake. (a) Fabrication process of electrode A. (b) Top view of the EA brake. (c) Section view of the EA brake.

from (8) and (9)

$$K_{\text{model}} = \sqrt{\frac{2d^2}{\mu \varepsilon_r \varepsilon_0 A}}. \tag{13}$$

By experiments we compared the response time and accuracy of open-loop control (only the feedforward control), PID control, and PID with feedforward control through experiments on the tensile testing machine (see Section IV). The PID controller might not be the optimal controller, but it can fulfill the current need in practice.

## III. Fabrication and Assembly

### A. EA Brake

During the fabrication, first, a piece of a composite film made by an aluminum layer (Al, 25 $\mu$m) and a Polyethylene terephthalate layer (PET, 25 $\mu$m) was located on a basement evenly [see Fig. 5(a)]. Then, dielectric paste (Luxprint, 8153, Dupont, the relative dielectric constant: 35) was uniformly coated on the surface (aluminum side) of the Al-PET film using a squeegee. The film was dried at 130°C for 1.25 hours [see Fig. 5(a)]. After cooling down for 1.25 h, the film was taken out and cut into a smaller piece (10 cm $\times$ 5 cm) as an electrode (Electrode A) of the EA brake. The thickness of the dielectric layer was approximately 34 $\mu$m, measured by a micrometer. We directly cut a piece from an Al-PET film with the size of 23 cm $\times$ 4.5 cm as the other electrode (electrode B) [see Fig. 5(b)]. The two electrode films (electrodes A and B) were finally encapsulated by a sleeve made from paper and polyimide to allow linear movement only [see Fig. 5(c)].

The whole EA brake weighs only 5.5 g and measures 0.76 mm in height and 65 mm in width. The coefficient of friction in this article is about 0.18.

### B. So-EAGlove

We integrated the EA brake into the So-EAGlove to generate soft perception on fingers (see Fig. 6). Electrode A was fixed to a wrist belt. One edge of electrode B was connected to an "O" shaped handle by a connector and a load cell (DYZ-100, Bengbu Da Yang). Here for conciseness, we decide to study the force feedback only on the two representative fingers (the index finger and the thumb). Thus, the handle accommodated three fingers (the index, middle, and ring fingers), and with the same structure, these fingers can be independent in the future design. A pulley (made from a smooth circular acrylic rod) on a rigid frame fixed to the thumb (as grounding) was used to change the direction of electrode B. The other edge of electrode B was attached to a sliding block.

The sliding block was connected to the wrist band by two low stiffness springs (10 N·m) made of rubber threads. The springs can pull back the brake to its original position and generate a weak pressing contact force on the fingertips, while the fingers release. The retracting force from the springs is neglected in the control model to save calculation time. Since the spring force is relatively weak (e.g., 10 N·m for each spring, only 0.1% of the maximum simulated stiffness 10 000 N·m), it is regarded as a disturbance and compensated by the closed-loop control system, which is displayed in detail in the experimental section.

A sensor (HG-C1200, Panasonic) installed on the forearm by a belt acquired the displacement of electrode B. The wrist belt is likely to deform and slip during the operation, resulting in errors in the displacement sensing. Based on our tests, the error magnitude is acceptable at this stage. The movement of the wrist during the operation also affects the displacement measurement. Thus, we asked the users to keep the wrist fixed during the operation. These problems regarding the displacement measurement can be solved in the future by integrating the sensor into the glove to sense the motion of the fingers directly.

The glove measures 20-cm long, 7-cm wide, and 12-cm high and weighs only 51 g. The maximum displacement of the figure tips is 60 mm.

Compared with the traditional variable stiffness haptic gloves [9], [15]–[18], [27], the primary advantages of this haptic glove are as follows (see Table I). First, it is lightweight (only 51 g), which reduces the fatigue of human hands and distraction resulting from the device's weight on the hand during VR operation. Second, the power consumption is extremely low (only 2.43 mW, mentioned in Section IV), which allows for a smaller battery or longer battery life. Third, the cost of the core component (EA brake) is only approximately \$8, which is much lower than a servo dc motor. Finally, the EA brake is intrinsically safe since the resisting force of the EA brake is passive, and it becomes zero if no motion is generated by the fingers. With the above advantages, this glove sacrifices the force feedback during

This article has been accepted for inclusion in a future issue of this journal. Content is final as presented, with the exception of pagination.



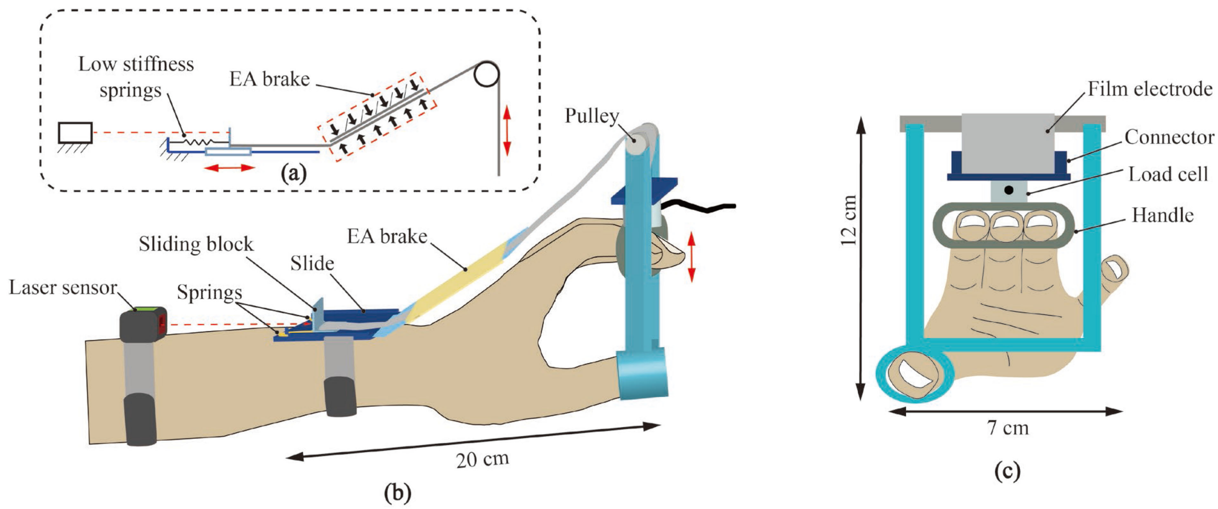


Fig. 6. Mechanical design of So-EAGlove. (a) Mechanical sketch. (b) Front view of So-EAGlove. (c) Side view of So-EAGlove.

TABLE I
COMPARISON WITH OTHER DEVICES

| | **Wolverine** [18] | **DextrES** [15] | **HIRO III** [9] | **CLAW** [16] | **Dexmo** [17] | **DESR** [27] | **So-EAGlove (this work)** |
|---|---|---|---|---|---|---|---|
| **Force feedback** | Constant stiffness | | Variable stiffness | | | | |
| **Actuation method** | One-way brake driven by a DC motor | EA brake (on/off force) | DC motor | | | Electroactive polymer | EA brake (tunable force) |
| **Weight (g)** | 55 | 8 (only brake) | 900 | 420 | 300 | 38 | 51 |
| **Range of motion** | 20-160 mm | Full hand closing | Thumb: 705, other: 587 $cm^3$ | 45 deg of the index finger | Full hand closing | 5 mm stroke | 60 mm stroke |
| **Max force to per finger (*N*)** | 106 | 20 | 3.6 | 30 | 0.5 Nm | 7.2 | 10* |
| **Average power consumption (mW)** | 290** | Less than 100 | - | More than 150 | 1000 | - | 2.43 |

*This value is calculated from the net maximum force (30 N) on the handler (for three fingers) acquired by the load cell.
**The average power is under the condition of running once every 3 seconds.

the pulling back of the fingers since the EA clutch itself can only generate a unidirectional braking force.

Contrasting to the previous haptic gloves integrating an EA brake [15], this prototype can generate a tunable resisting force to simulate a larger range of objects. Furthermore, the resisting force direction is guided by a frame to be vertical to the fingertips in this prototype, same as the reacting force direction of a real object, to improve the realistic feeling, while the force direction of the previous prototype is lateral [15]. This article mainly focuses on the softness sensation on the two representative fingers of the thumb and index finger, since they are the two primary fingers involving daily activities [28]. Currently, the middle and ring fingers share the same handle with the index finger, but they can be independent in the future with the same mechanism and design.

### C. Electrical Circuit

The electrical design is shown in Fig. 7. When the fingertips move, their displacement and force are acquired by the distance

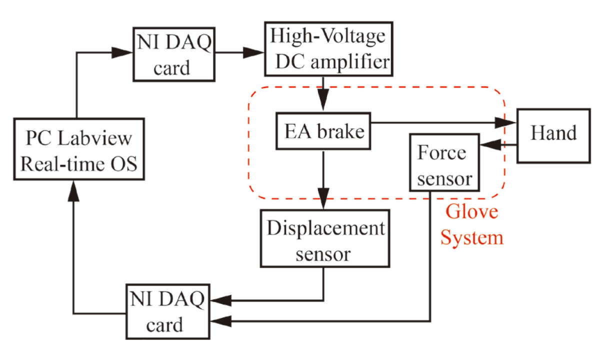


Fig. 7. Electrical design block diagram.

and force sensors, respectively, and sent to a DAQ board (4330, NI). These data are analyzed by a LabVIEW program based on the aforementioned control method, and the DAQ board outputs the control voltage. After being amplified by 200 times (Model 615-10, Trek), high voltage is supplied to the electrodes of the EA brake.

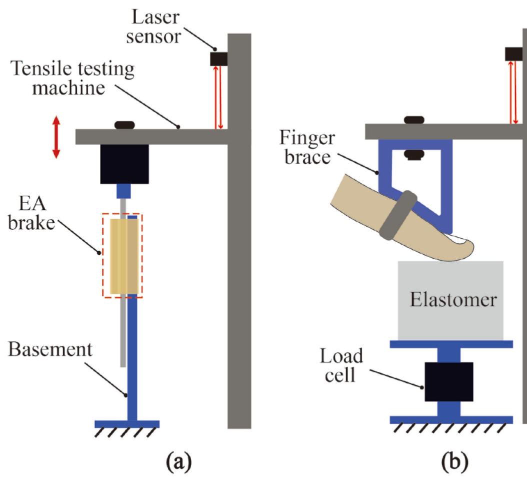


Fig. 8. Experimental setups on the tensile testing machine. (a) Braking force test. (b) Preliminary test for the contact model parameters.

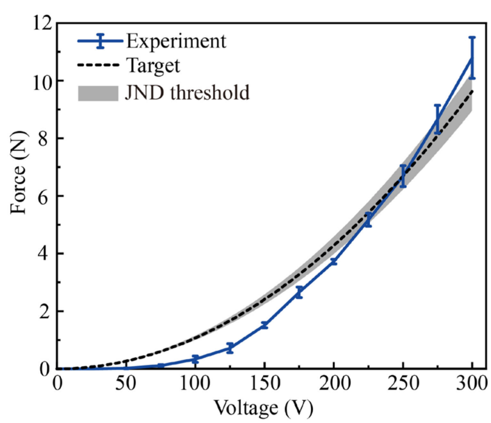


Fig. 9. EA braking force by open-loop control.

## IV. Experimental Results

### A. Characterization of the EA Brake

*1) Braking Force:* To measure the EA braking force, we fixed electrode A to the movable stage of a universal tensile testing machine (ZQ-990B, ZHIQU) through a load cell (ZQ-770-10, ZHIQU) and Electrode B to the basement [see Fig. 8(a)]. While the EA brake was pulled at 30 mm/min, the load cell acquired the braking force. We kept the applied voltage below 300 V since the applied voltage higher than 350 V was more likely to cause an electrical breakdown. At each condition, at least three trials were conducted.

As shown in Fig. 9, the experimental data of braking force share the same tendency with the estimation based on (8) and (9). In the estimation, $K_{\text{model}}$ is calculated based on (13). The dielectric thickness $d$ in the estimation was calculated from (8) after achieving the adhesive force in a preliminary test. The average magnitudes of the experimental results have a large discrepancy with the target, even out of the JND threshold (the gray area in Fig. 9), perhaps due to the variable air gap between the two electrode films and the nonlinear material properties. This is unacceptable for this haptic feedback device since the subject can feel the force difference, and hence, the closed-loop control is necessary.

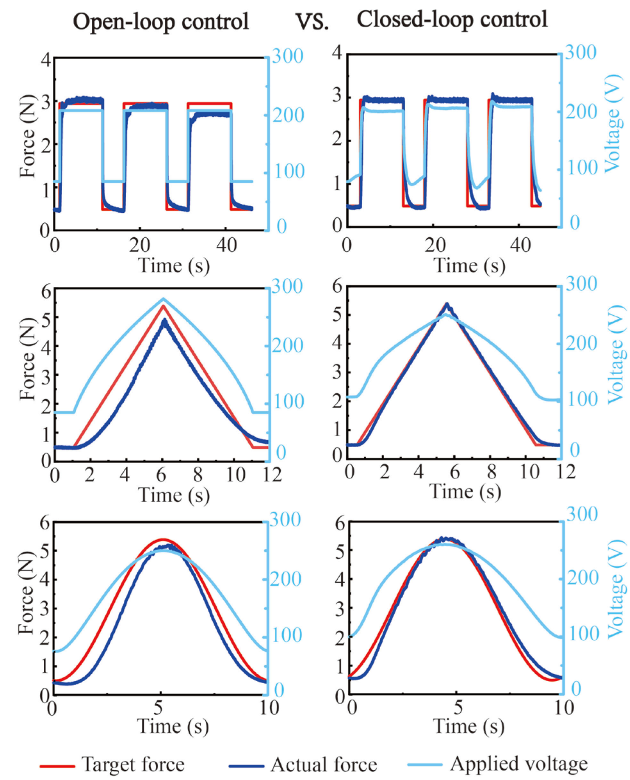


Fig. 10. Comparison between open-loop control and closed-loop control while following a square wave, a triangle wave, and a sine wave, respectively.

*2) Closed-Loop Control:*

*a) Force Magnitude Control:* Here, we compare the performance of the conventional open-loop control and the PID closed-loop control. We acquired the force data in Fig. 10 using the experimental setup (a tensile testing machine) in Fig. 8(a). The force was measured when the EA brake was pulled to move linearly at a constant speed. The closed-loop controller generates a force following the aim waveforms accurately, as shown in Fig. 10. For example, while simulating square, triangle, and sinusoidal force waves, the mean absolute error is 4.41%, 22.7%, and 20.7% by an open-loop control, and 0.52%, 7.11%, and 9.89% by closed-loop control, respectively. The closed-loop control improved the accuracy by approximately three times.

*b) Response Time:* The response time is a system constant, and it does not change with the input signal (voltage). However, when the feedback is added to the open-loop system, the system is changed, and then the response times can be improved [29]. With the method same in the last part, we tested the transient response of the EA brake. Here, we select the activation voltage as 210 V. As shown in Fig. 11, with the open-loop controller, the rise time of the braking force is approximately 50 ms, and the fall time 87 ms. Under the closed-loop control with feedforward (PID with feedforward), the force can change to the aim force more quickly, as shown in Fig. 11, with the rise time of only 38 ms (24% shorter) and the fall time of 68 ms (22% shorter). Under the proposed control, the applied voltage is the feedback

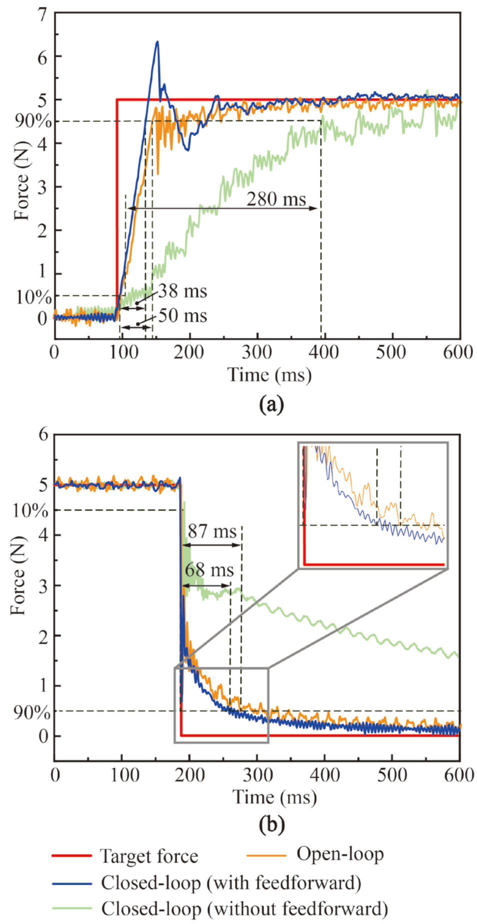


Fig. 11. Comparison of the transient responses between the open-loop, the closed-loop without feedforward and the closed-loop with feedforward. (a) Rise time. (b) Fall time.

voltage ($u_{ff}$) together with the feedforward voltage ($u_{fb}$), which can be higher than the open-loop input signal (only $u_{ff}$), but has the same target force, resulting in a shorter response time [30]. The response time is adequate for the haptic device since the human response time is approximately 235 ms [31]. However, if we use the closed-loop control without feedforward (simple PID), the rise and fall times are much longer (280 ms and over 400 ms), which is unacceptable. The errors of PID and PID with feedforward are 4.78% and 1.63%, respectively, smaller than the JND and acceptable currently in this device.

*c) Elastic Object Rendering:* For ideal elastic objects, the contact force is proportional to the corresponding deformation, just like a spring. We use the tensile machine to simulate the compressing process of a human finger (at a constant speed of 30 mm/min), and the EA brake resists the "finger" by the braking force. In the test, the EA brake can generate a braking force that increases linearly with the displacement, just like the target (absolute average error: 4.1%) [see Fig. 12(a)]. The stiffness of the linear braking force ranges from 1 to 10000 N·m, corresponding to Young's modulus of a virtual ideal elastic object ranging from 540 Pa to 5.4 MPa according to (1) (here $L$ is 60 mm considering the distance from the index finger to the thumb finger, and $S$ is 110 mm$^2$ considering the contact area

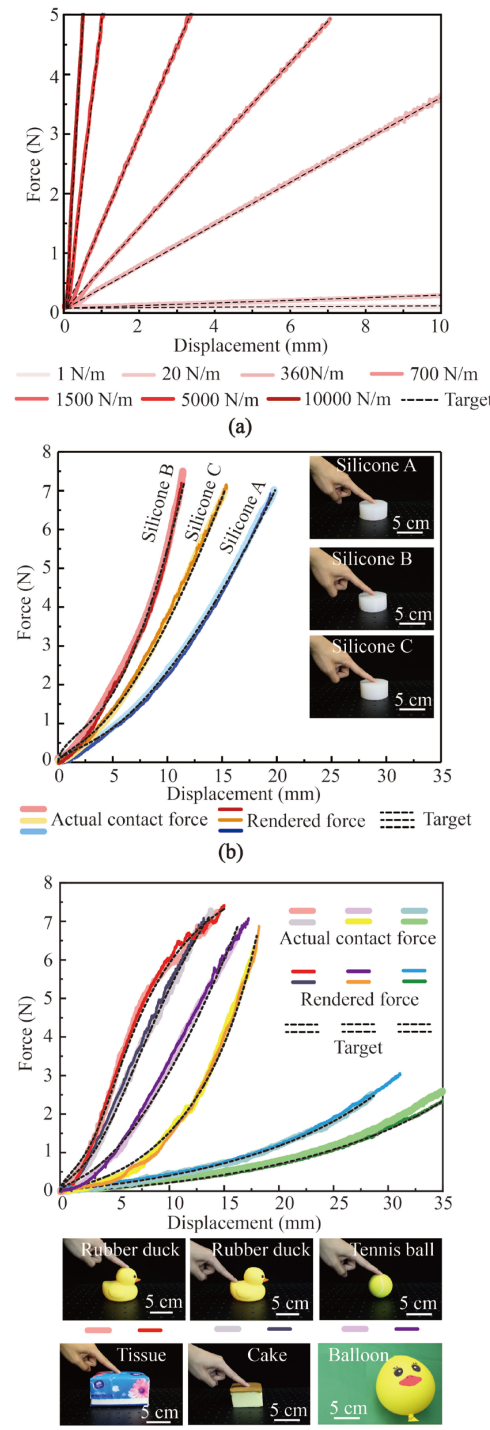


Fig. 12. Contact force simulated by the EA brake. (a) Contact force on springs. (b) Contact force on silicone blocks. (c) Contact force on different complex soft objects.

of the finger pad [32]). This means that the So-EAGlove can simulate a large range of objects [33]–[39] (see Fig. 1).

For nonlinear elastic objects, the contact force increases nonlinearly with the deformation, and multiple parameters are involved in the model, as shown in (2) and (7). We made three elastic samples from silicone A (HY-E600, HONGYEJIE),

TABLE II
MODEL PARAMETERS

| Objects | $E_{o1}$ (Pa/N) | $E_{o2}$ (Pa) | $v_0$ | $c$ (Ns/m$^{3/2}$) |
|---|---|---|---|---|
| HY-E610 | 1557 | 23290 | 0.486 | 24540 |
| HY-E600 | 268 | 12220 | 0.492 | 11230 |
| HY-E605 | 211 | 19900 | 0.483 | 16140 |
| Rubber duck head | -9862 | 92910 | 0.486 | 25640 |
| Rubber duck tail | -3836 | 55520 | 0.1023 | 19448 |
| Tennis ball | 200 | 18660 | 0.47 | 11300 |
| Tissues | 1798 | 8921 | 0.2635 | 4600 |
| Cake | 653 | 2010 | 0.116 | 2740 |
| Balloon | 394 | 1180 | 0.485 | 540 |

silicone B (HY-E610, HONGYEJIE), and silicone C (HY-E605, HONGYEJIE), respectively. To measure the contact model parameters of these prototypes, we pushed a finger by the moving stage of a tensile testing machine (ZQ-990B, ZHIQU) on the objects at a constant speed (30 mm/min) and acquired the contact force and displacement by a load cell (ZQ-770-10, ZHIQU) and a displacement sensor (HG-C1200, Panasonic), respectively [see Fig. 8(b)]. We fit (nonlinear least squares) the contact force data by the contact model and achieved the parameters (see Table II). Based on these parameters, we created the target curvatures for these three samples, respectively, [see Fig. 12(b)]. Then we controlled the EA braking force with the closed-loop control method to follow the target curvatures. As shown in Fig. 12(b), little discrepancy (absolute average error: 3.5%) occurs between the force curvatures of the real and the virtual objects. In addition to the simple soft blocks, with a similar method, the EA brake can simulate the contact force of complex objects, such as a rubber duck, a tennis ball, a tissue stock, a piece of cake, and a balloon, as shown in Fig. 12(c), since the complex objects can be simplified into equivalent simple soft blocks predictable by the model in this article [20], [40]. The absolute average errors are smaller than 5.68%. Therefore, the EA brake is adequate to simulate elastic objects.

## B. Experiments on the Desktop Platform

*1) Desktop Platform:* The performance of haptic gloves is dominated by the finger contact force, but also influenced by sounds, the weight of the glove, and the touching force on the glove to the wrist [41]. To characterize the performance of the EA brake during the interaction with human beings and eliminate the other influences, we built up a desktop platform, as shown in Fig. 13(a) and (b), in which only the participant's fingers contact the device. Film A of the EA brake was dragged by the fingers instead of a universal tensile testing machine. Film B was installed on the frame through a load cell (ZQ-770-10, ZHIQU). A reflector was fixed to Film A, and its displacement was acquired by a laser displacement sensor (HG-C1200, Panasonic). The electrostatic braking force was controlled by the closed-loop controller.

*2) Elastic Object Rendering:* On the desktop platform, we reproduced the force of ideal and non-linear elastic objects, respectively, while the participants were asked to push the EA brake down. At each condition, three trials were conducted. As shown in Fig. 13(c) and (d), the force curvatures of the virtual objects possess similar tendencies with the aim profiles. The absolute average error is 6.6% for ideal elastic objects and 7.0% for nonlinear elastic objects. The errors are smaller than the JND (7%), still acceptable for the haptic glove. These errors are larger compared with the force generated on the tensile machine, perhaps resulting from that the fingertips moved at a variable speed during the test, and the coefficient of friction non-linearly changed with speed [42]. The nonlinearity of the coefficient of the friction results in more errors on the electrostatic adhesive force. That is why the simulated force pushed by the fingers possessed a larger error compared with the one pulled by the machine.

*3) Subjective Test:*

*a) Correction of Different Stiffness:* To verify the feasibility of the simulated force and stiffness, we chose three stiffness (30 m, 75, and 120 N·m, corresponding to low stiffness, medium stiffness, and high stiffness) for the subjective test. A total of four participants (one female and three male) attended the test, and all participants were right-handed and 20–26 years old. All the experiments in this article were approved by the Southern University of Science and Technology, Human Participants Ethics Committee (20210090), and consent was obtained from all participants.

First, low stiffness, medium stiffness, and high stiffness were simulated by the EA brake, respectively, and participants were trained to press the virtual springs until they could correctly distinguish the three levels of stiffness. Then the test was started, while each participant was blindfolded and had the ears blocked by earplugs. We conducted the test 30 times, including 10 times for each stiffness level, and these three levels were randomly mixed. After each test, the participant was asked, "Is the stiffness of this simulated spring low, medium, or high?". The answers and real stiffness were recorded [see Fig. 13(e)].

The results show a significant influence of simulated stiffness on participants' answers ($\chi^2(2) = 90.143$, $p<0.001$, Kruskal–Wallis nonparametric test), and there is a statistically significant difference between each two of the low, medium, and high stiffness groups ($p<0.001$). The correct selection rate is 81.6% on the desktop platform. This means the platform can generate the proper force for different stiffness objects and subjects can differ different stiffness or softness simulated by the EA brake.

*b) Realism Test of the Simulated Spring:* We tested the realism of the simulated spring by another subjective test. 25 volunteers (24 male and 1 female) participated in the trial. All participants were 20–29 years old, and one of them was left-handed. When they were tested, they were blindfolded, and their ears were blocked. Each participant was tested 12 times (6 times for the real spring and 6 times for the simulated spring, and they were randomly mixed). The participants did not know the content of the test in advance. When the participants were tested on the simulated spring (stiffness 120 N·m), the EA brake was controlled by the aforementioned closed-loop control method. Since the realism test is subjective and susceptible to psychological effects, we introduced a real spring

This article has been accepted for inclusion in a future issue of this journal. Content is final as presented, with the exception of pagination.



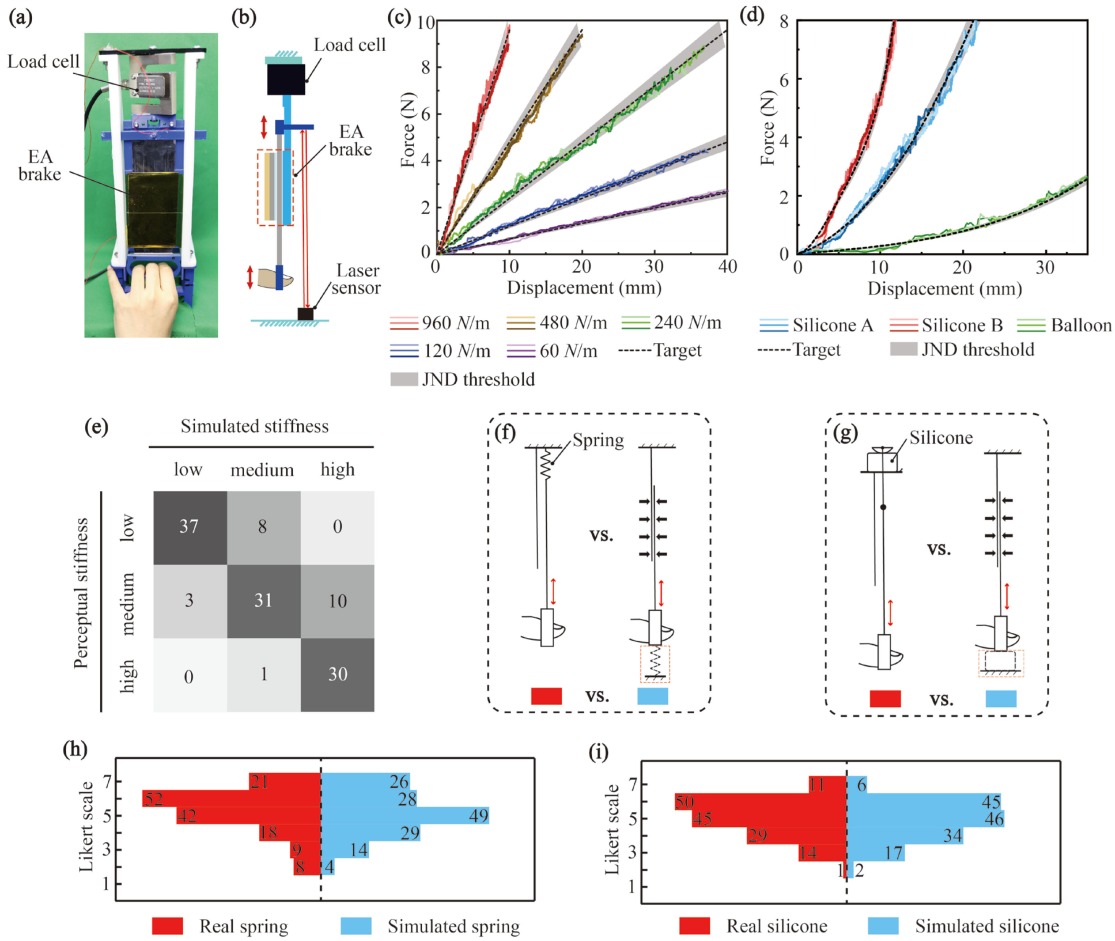


Fig. 13. Experiments on the desktop platform. (a) Experimental setup. (b) Schematic diagram of the experimental setup. (c) Results of simulating springs of different stiffness. (d) Results of simulating non-linear elastic objects. Three trials were conducted for each condition. (e) Correction diagram for different simulated stiffness. (f) Schematic diagram of the experimental setup for realism test of the simulated spring and the real spring. (g) Schematic diagram of the experimental setup for realism test of simulated silicone and real silicone. (h) Participants' answers to the realism test for springs. (i) Participants' answers to the realism test for silicone. The length of the rectangle and the number on the rectangle represent the selected frequency of participants.

as a reference in the trial. When the participants were tested on the real spring (stiffness 120 N·m), we cut off the power of the EA brake and connected the real spring to the sliding block and base plate [see Fig. 13(f)]. After each test, the participants were asked, "Is this a spring?." Participants were rated using the Likert seven-point scale (seven-strongly agree, six-agree, five-relatively agree, four-uncertain, three-relatively disagree, two-disagree,and one-strongly disagree).

The answers of participants are shown in Fig. 13(h). The absolute values of the realism level for the virtual spring and the real spring are susceptible to psychological effects, and hence here, we focus more on their ratio. In the tests, the overall average realism level for the simulated spring (5.07, i.e., relatively agree it is spring) is 96.9% of that (5.23) for the real spring. Moreover, there is no statistically significant difference between the subjective feelings of the two groups of the real spring and the simulated spring ($p = 0.150$, Mann–Whitney U test). It means the participants cannot distinguish the virtual spring from the real counterpart. Therefore, using the EA brake on the desktop platform, we can generate a virtual spring with high-level realism.

*c) Realism Test of the Simulated Silicone:* We also tested the realism of the simulated silicone (HY-E600). 25 volunteers (all male) participate in the test. All participants were 20–29 years old and right-handed. When they were tested, they were blindfolded, and their ears were blocked. Each participant was tested by 12 times (in which 6 times for the real silicone and 6 times for the simulated silicone were randomly mixed), and participants did not know the content of the test in advance. When the participants were tested by the real silicone, we cut off the power of the EA brake and put the silicone cylinder inside of the device [see Fig. 13(g)]. When the fingers pressed down, the silicone cylinder was squeezed, and the force was transmitted to the fingertips by a rope. After each test, the participants were asked, "Is this silicone?." Participants rated the answer on the Likert seven-point scale.

The answers of participants are shown in Fig. 13(i). The overall average realism level for the simulated silicone (4.89) is 96.3% of that for the real silicone (5.08). The statistical difference between the real and the simulated silicone is little ($p = 0.146$). It means the simulated silicone was hard to be identified from the real silicone by the participants. Therefore, the realism

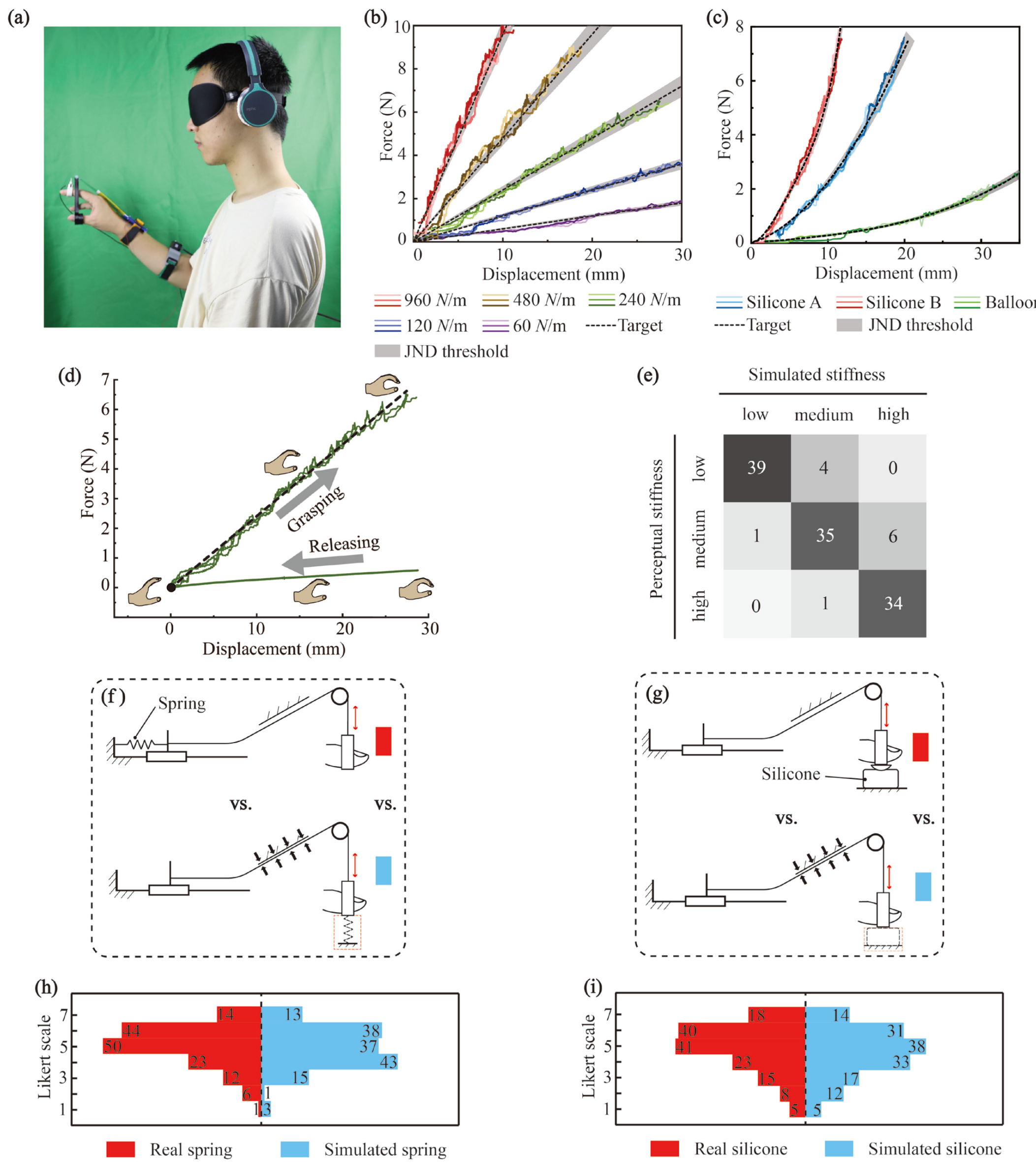


Fig. 14. Experiment on the glove. (a) So-EAGlove worn on human hand. Objective tests: (b) Results of simulating springs of different stiffness. (c) Results of simulating non-linear elastic objects (three trials were conducted for each condition). (d) Finger contact force in the grasping and releasing process (the green solid line represents the experimental data, and the dashed line displays the aim trajectory). Subjective tests: (e) Correction diagram for different simulated stiffness. (f) Schematic diagram of the experimental setup for realism test of the simulated spring and the real spring. (g) Schematic diagram of the experimental setup for realism test of simulated silicone and real silicone. (h) Participants' answers to the realism test for springs, and (i) participants' answers to the realism test for silicone (the length of the rectangle and the number on the rectangle represent the selected frequency of participants).

of the simulated elastomer is acceptable. We conducted the subjective tests by following similar protocols in [43]. Moreover, to improve the objectivity of subjective testing, we introduced a control group (real springs and silicones) to eliminate subjective bias.

## C. Experimental Results on So-EAGlove

*1) Characterization:* We finally tested the performance of So-EAGlove on subjects' hands, as shown in Fig. 14(a). The thumb was fixed in the thumb ring, and other fingers were fixed on the handle. When the fingers squeezed the virtual objects, the simulated force and displacement were recorded. At each condition, three trials were conducted.

As shown in Fig. 14(b) and (c), the force measured on the So-EAGlove are more fluctuant than those acquired on the desktop platform, especially while simulating the strong springs (e.g., 960 and 480 N·m). The absolute average error is 6.24% for ideal elastic objects and 5.22% for nonlinear elastic objects, which is still under the JND threshold and acceptable. The force error perhaps is because the electrode films were fixed on a compliant belt on the arm (might deform and slip during the operation) and supported by the pulley (causing more friction force that is non-linear to the speed).

We also tested the force while the fingers retract [see Fig. 14(d)]. In this procedure, the EA brake was powered OFF. Only the small-stiffness springs pulled back the fingertips and generated a contact force, which can promote a realistic feeling.

*2) Subjective Test:*

*a) Correction of Different Stiffness:* To verify the feasibility of the So-EAGlove simulating different stiffness objects, we conducted experiments similar to that introduced in the last part [see Section IV-B]. A total of four participants (3 male and 1 female, 23–25 years old, all right-handed) participated in the test. Their answers and the stiffness of simulated springs were recorded.

The results (see Fig. 14(e)) show a significant influence of simulated stiffness on participants' answers ($\chi^2(2) = 102.594$, $p<0.001$, Kruskal–Wallis nonparametric test). Any one of the three groups (low stiffness, medium stiffness, and high stiffness) is statistically different from the others ($p<0.001$, Mann–Whitney U test). The correct selection rate on the glove is 90%. Thus, the So-EAGlove is capable of simulating different stiffness. Moreover, the glove generated a higher correct rate than the desktop platform did in our tests, perhaps because the forearm of the participants could also feel the force feedback through the wrist belt during the glove test, and more skin area resulted in higher sensitivity to the force and stiffness variation.

*b) Realism Test of the Simulated Spring:* We tested the realism of the virtual spring (120 N·m) simulated by the So-EAGlove with the same method as that on the desktop platform. 25 participants (24 male and 1 female, 20-25 years old) joined in the test. We collected the subjective feedback of the participants on the real and the simulated spring, respectively, [see Fig. 14(f)].

As shown in Fig. 14(h), the overall average realism level for the simulated spring (4.84) is 96.4% of that for the real spring (5.02). There is no statistically significant difference between the two groups ($p = 0.143$, Mann–Whitney U test). The participants can hardly distinguish the simulated spring from the real spring, and thus the realism is acceptable.

*c) Realism Test of the Simulated Silicone:* We also test the realism of the simulated silicone (HY-E600). We put a real silicone cylinder under the handle and three-dimensional printed fingertip [see Fig. 14(g)] to generate real silicone-contact force for human fingers and simulate the same force curvature by the EA brake. 25 participants (22 male and 3 female, 19–29 years old, all right-handed) participated in the test. The experimental procedure is the same as that on the desktop platform.

As shown in Fig. 14(i), the overall average realism level for the simulated silicone (4.57) is 94.1% of that for the real silicone (4.86). There are no significant differences between the simulated silicone and the real silicone ($p = 0.074$).

Comparably, the realism level of the simulated objects on the glove is slightly lower than the value on the desktop platform, perhaps because the forearm under the wrist belt of the haptic glove felt more interacting forces and made the participants more sensitive to the force difference.

*3) Power Consumption and Safety:* To measure the power consumption of the So-EAGlove, we connected a resistor (1 M$\Omega$) in series with the EA brake of the So-EAGlove. We measured the power in two ways. On the first way, the power

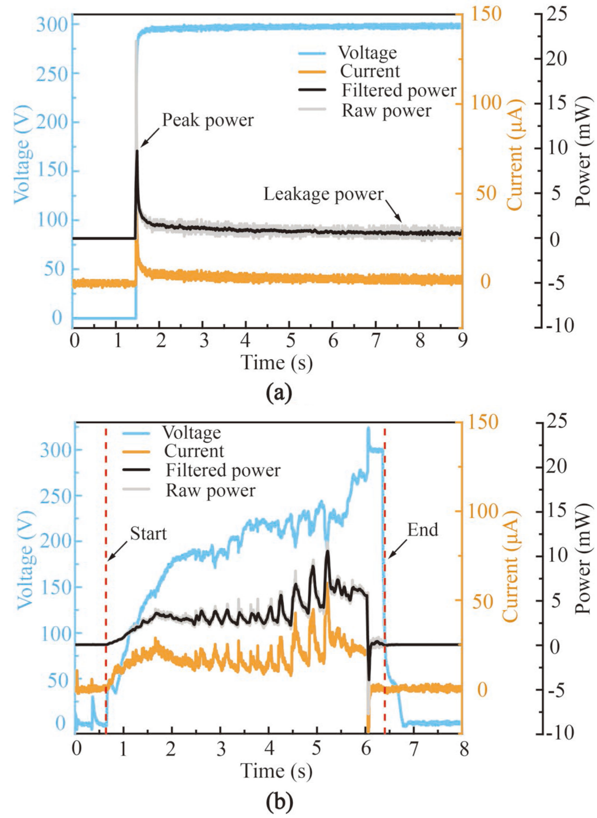


Fig. 15. Power consumption. (a) Applied voltage is constant and the EA brake is static. (b) EA brake of the So-EAGlove is dragged by human hand and it is simulating a virtual spring.

consumed was measured when the voltage was turned on and then kept constant (300 V). When the voltage was on, the current and voltage rose rapidly [see Fig. 15(a)]. The peak power was approximately 10 mW. Then, the current declined to a shallow value (leakage current) in 1 s, and the power remained at a very low level (leakage power, 0.58 mW).

By the second way, the power consumption was measured when the EA brake was subjected to a dragging force in the So-EAGlove, and the EA braking force was simulating a virtual spring (240 N·m stiffness). When the hand began to press the handle of the So-EAGlove, the target force increased with the pressing distance, controlled by the closed-loop controller. The current and voltage also increased gradually [see Fig. 15(b)]. In this article model, the average power is 2.43 mW. The So-EAGlove can work for 86.4 h (more than three days) continuously at this output power with only a button battery (A76, NANFU, 140 mAh, 2 g). Currently, the high voltage amplifier is OFF-board. The amplifiers can be made portable in the future, by utilizing the similar technique in the literature [44].

Although with high voltage, the glove is expected to be safe enough. First, the electrodes are all encapsulated by dielectric materials [see Fig. 5(c)] to prevent electric shock. Second, a large current is more dangerous than high voltage to human beings [45]. High voltage devices were already used in the medical field, which requires extremely high safety (e.g., electrosurgery uses voltages of more than 500 V) [46]. The working current (less than100 $\mu$A) of the glove is much smaller than the current threshold of human perceptibility (1 mA) [47].

## V. Conclusion

In this article, So-EAGlove– a VR haptic glove rendering softness sensation has been presented by integrating a force-tunable EA brake. We built the EA force model and the closed-loop control model of the EA brake and devised a prototype with only 51 g weight and 2.43 mW power consumption. Tested on a universal tensile machine, the desktop platform, and So-EAGlove, respectively, the simulated force can be controlled accurately (absolute average error smaller than 7%, within the JND threshold). The subjective tests also verify that So-EAGlove can generate a high realism feeling.

Currently, the accessory components are all off-board, and the So-EAGlove only allows three fingers (the index, middle, and ring fingers) to operate together. In the future, we will improve its portability by integrating the voltage amplifier, microcontroller, stretchable sensors, and a battery on the glove. To achieve more diverse functions and more dexterity, we will split the current plane EA brake into independent and narrow ones (perhaps with multiple layers for stronger force) to fit the fingers, upgrade the supporting frame to guide the force of EA brakes, and independently control the contact force on each finger. The fixture structure will be improved to fit fingers in a larger range of sizes. Moreover, with the same technique, we will render objects with more complex material properties, e.g., anisotropy and hysteresis. A VR glass is planned to combine into this system to strengthen the realism and immersion feeling of the subjects. Other advanced control algorithms will be introduced and evaluated to improve control accuracy and stability.

## Acknowledgment

The authors acknowledge the assistance of SUStech Core Research Facilities.

## References


[1] G. Di Gironimo, A. Lanzotti, and A. Vanacore, "Concept design for quality in virtual environment," *Comput. Graph.*, vol. 30, no. 6, pp. 1011–1019, 2006.

[2] T. S. Mujber, T. Szecsi, and M. S. J. Hashmi, "Virtual reality applications in manufacturing process simulation," *J. Mater. Process. Technol.*, vol. 155, pp. 1834–1838, 2004.

[3] E. A.-L. Lee and K. W. Wong, "A review of using virtual reality for learning," *Trans. edutainment I. Lecture Notes Comput. Sci.*, vol. 5080, pp. 231–241, 2008.

[4] A. Rizzo *et al.*, "Virtual reality goes to war: A brief review of the future of military behavioral healthcare," *J. Clin. Psychol. Med. Settings*, vol. 18, no. 2, pp. 176–187, 2011.

[5] L. Rebenitsch and C. Owen, "Review on cybersickness in applications and visual displays," *Virtual Real,* vol. 20, no. 2, pp. 101–125, 2016.

[6] M. A. Srinivasan and C. Basdogan, "Haptics in virtual environments: Taxonomy, research status, and challenges," *Comput. Graph.*, vol. 21, no. 4, pp. 393–404, 1997.

[7] C. Pacchierotti, S. Sinclair, M. Solazzi, A. Frisoli, V. Hayward, and D. Prattichizzo, "Wearable haptic systems for the fingertip and the hand: Taxonomy, review, and perspectives," *IEEE Trans. Haptics*, vol. 10, no. 4, pp. 580–600, Oct.–Dec. 2017.

[8] S. Das, Y. Kishishita, T. Tsuji, C. Lowell, K. Ogawa, and Y. Kurita, "Force-Hand glove: A wearable force-feedback glove with pneumatic artificial muscles (PAMs)," *IEEE Robot. Autom. Lett.*, vol. 3, no. 3, pp. 2416–2423, Jul. 2018.

[9] T. Endo *et al.*, "Five-fingered haptic interface robot: HIRO III," *IEEE Trans. Haptics*, vol. 4, no. 1, pp. 14–27, Jan.–Mar. 2011.

[10] J. Blake and H. B. Gurocak, "Haptic glove with MR brakes for virtual reality," *IEEE/ASME Trans. Mechatronics*, vol. 14, no. 5, pp. 606–615, Oct. 2009.

[11] H. Wang, A. Yamamoto, and T. Higuchi, "A crawler climbing robot integrating electroadhesion and electrostatic actuation," *Int. J. Adv. Robot. Syst.*, vol. 11, no. 12, 2014, Art. no. 191.

[12] H. Wang and A. Yamamoto, "Analyses and solutions for the buckling of thin and flexible electrostatic inchworm climbing robots," *IEEE Trans. Robot.*, vol. 33, no. 4, pp. 889–900, Aug. 2017.

[13] J. Shintake, S. Rosset, B. Schubert, D. Floreano, and H. Shea, "Versatile soft grippers with intrinsic electroadhesion based on multifunctional polymer actuators," *Adv. Mater.*, vol. 28, no. 2, pp. 231–238, 2016.

[14] E. Leroy, R. Hinchet, and H. Shea, "Multimode hydraulically amplified electrostatic actuators for wearable haptics," *Adv. Mater.*, vol. 32, no. 36, 2020, Art. no. 2002564.

[15] R. Hinchet, V. Vechev, H. Shea, and O. Hilliges, "Dextres: Wearable haptic feedback for grasping in vr via a thin form-factor electrostatic brake," in *Proc. 31st Annu. ACM Symp. User Interface Softw. Technol.*, 2018, pp. 901–912.

[16] I. Choi, E. Ofek, H. Benko, M. Sinclair, and C. Holz, "Claw: A multifunctional handheld haptic controller for grasping, touching, and triggering in virtual reality," in *Proc. CHI Conf. Hum. Factors Comput. Syst.*, 2018, pp. 1–13.

[17] X. Gu, Y. Zhang, W. Sun, Y. Bian, D. Zhou, and P. O. Kristensson, "Dexmo: An inexpensive and lightweight mechanical exoskeleton for motion capture and force feedback in vR," in *Proc. CHI Conf. Hum. Factors Comput. Syst.*, 2016, pp. 1991–1995.

[18] I. Choi, E. W. Hawkes, D. L. Christensen, C. J. Ploch, and S. Follmer, "Wolverine: A wearable haptic interface for grasping in virtual reality," in *Proc. IEEE/RSJ Int. Conf. Intell. Robots Syst.*, 2016, pp. 986–993.

[19] I. Yoshiaki, "Display of soft elastic object by simultaneous control of fingertip contact area and reaction force," *Trans. Virtual Real. Soc. Jpn.*, vol. 9, no. 2, pp. 1–8, 2004.

[20] M. Machado, P. Moreira, P. Flores, and H. M. Lankarani, "Compliant contact force models in multibody dynamics: Evolution of the Hertz contact theory," *Mech. Mach. Theory*, vol. 53, pp. 99–121, 2012.

[21] X.-D. Pang, H. Z. Tan, and N. I. Durlach, "Manual discrimination of force using active finger motion," *Perception Psychophysics*, vol. 49, no. 6, pp. 531–540, 1991.

[22] A. Johnsen and K. Rahbek, "A physical phenomenon and its applications to telegraphy, telephony, etc.," *J. Inst. Elect. Eng.*, vol. 61, no. 320, pp. 713–725, 1923.

[23] J. Guo, J. Leng, and J. Rossiter, "Electroadhesion technologies for robotics: A comprehensive review," *IEEE Trans. Robot.*, vol. 36, no. 2, pp. 313–327, Apr. 2020.

[24] J. Guo, M. Tailor, T. Bamber, M. Chamberlain, L. Justham, and M. Jackson, "Investigation of relationship between interfacial electroadhesive force and surface texture," *J. Phys. D. Appl. Phys.*, vol. 49, no. 3, 2015, Art. no. 35303.

[25] T. Nakamura and A. Yamamoto, "Modeling and control of electroadhesion force in DC voltage," *Robomech. J.,* vol. 4, no. 1, pp. 1–10, 2017.

[26] R. V. Grigorii and J. E. Colgate, "Closed loop application of electroadhesion for increased precision in texture rendering," *IEEE Trans. Haptics*, vol. 13, no. 1, pp. 253–258, Jan.–Mar. 2020.

[27] R. Zhang, P. Lochmatter, A. Kunz, and G. M. Kovacs, "Spring roll dielectric elastomer actuators for a portable force feedback glove," in *Proc. Smart Struct. Mater., Electroactive Polym. Actuators Devices*, 2006, pp. 505–516.

[28] I. M. Bullock, J. Z. Zheng, S. De La Rosa, C. Guertler, and A. M. Dollar, "Grasp frequency and usage in daily household and machine shop tasks," *IEEE Trans. Haptics*, vol. 6, no. 3, pp. 296–308, Jul.–Sep. 2013.

[29] K. Ogata, *Modern Control Engineering*, vol. 5, Saddle River, NJ, USA: Prentice Hall Upper, 2010.

[30] S. B. Diller, S. H. Collins, and C. Majidi, "The effects of electroadhesive clutch design parameters on performance characteristics," *J. Intell. Mater. Syst. Struct.*, vol. 29, no. 19, pp. 3804–3828, 2018.

[31] D. L. Woods, J. M. Wyma, E. W. Yund, T. J. Herron, and B. Reed, "Factors influencing the latency of simple reaction time," *Front. Hum. Neurosci.*, vol. 9, 2015, Art. no. 131.

[32] B. M. Dzidek, M. J. Adams, J. W. Andrews, Z. Zhang, and S. A. Johnson, "Contact mechanics of the human finger pad under compressive loads," *J. Roy. Soc. Interface*, vol. 14, no. 127, 2017, Art. no. 20160935.

[33] D. Rus and M. T. Tolley, “Design, fabrication and control of soft robots,” *Nature*, vol. 521, no. 7553, pp. 467–475, 2015.

[34] J. I. Garrido, J. E. Lozano, and D. B. Genovese, “Effect of formulation variables on rheology, texture, colour, and acceptability of apple jelly: Modelling and optimization,” *LWT-Food Sci. Technol.*, vol. 62, no. 1, pp. 325–332, 2015.

[35] C. Keetels, T. Van Vliet, and P. Walstra, “Relationship between the sponge structure of starch bread and its mechanical properties,” *J. Cereal Sci.*, vol. 24, no. 1, pp. 27–31, 1996.

[36] C. C. Ihueze and C. E. Mgbemena, “Design for limit stresses of orange fruits (Citrus sinensis) under axial and radial compression as related to transportation and storage design,” *J. Saudi Soc. Agriculture Sci.*, vol. 16, no. 1, pp. 72–81, 2017.

[37] A. Karimi, S. Kudo, R. Razaghi, and M. Navidbakhsh, “Measurement of the mechanical properties of the handball, volleyball, and basketball using DIC method: A combination of experimental, constitutive, and viscoelastic models,” *Sport Sci. Health*, vol. 11, no. 3, pp. 295–303, 2015.

[38] M. Grotte, F. Duprat, E. Piétri, and D. Loonis, “Young’s modulus, poisson’s ratio, and Lame’s coefficients of golden delicious apple,” *Int. J. Food Prop.*, vol. 5, no. 2, pp. 333–349, 2002.

[39] K. Tian, C. Shen, X. Li, J. Huang, Q. Chen, and B. Zhang, “Mechanical properties and compression damage simulation by finite element for kiwifruit,” *Int. Agric. Eng. J.*, vol. 26, no. 4, pp. 191–201, 2017.

[40] E. P. Scilingo, M. Bianchi, G. Grioli, and A. Bicchi, “Rendering softness: Integration of kinesthetic and cutaneous information in a haptic device,” *IEEE Trans. Haptics*, vol. 3, no. 2, pp. 109–118, Apr.–Jun. 2010.

[41] J. Yin, R. Hinchet, H. Shea, and C. Majidi, “Wearable soft technologies for haptic sensing and feedback,” *Adv. Funct. Mater.*, vol. 31, no. 39, 2021, Art. no. 2007428.

[42] J. T. Burwell and E. Rabinowicz, “The nature of the coefficient of friction,” *J. Appl. Phys.*, vol. 24, no. 2, pp. 136–139, 1953.

[43] I. Choi, H. Culbertson, M. R. Miller, A. Olwal, and S. Follmer, “Grabity: A wearable haptic interface for simulating weight and grasping in virtual reality,” in *Proc. 30th Annu. ACM Symp. User Interface Softw. Technol.*, 2017, pp. 119–130.

[44] B. Goldberg *et al.*, “Power and control autonomy for high-speed locomotion with an insect-scale legged robot,” *IEEE Robot. Autom. Lett.*, vol. 3, no. 2, pp. 987–993, Apr. 2018.

[45] H. Wang *et al.*, “Biologically inspired electrostatic artificial muscles for insect-sized robots,” *Int. J. Rob. Res.*, vol. 40, no. 6–7, pp. 895–922, 2021.

[46] D. Palanker, A. Vankov, and P. Jayaraman, “On mechanisms of interaction in electrosurgery,” *New J. Phys.*, vol. 10, no. 12, 2008, Art. no. 123022.

[47] R. M. Fish and L. A. Geddes, “Conduction of electrical current to and through the human body: A review,” *Eplasty*, vol. 9, pp. e44, 2009.

**Quan Xiong** received the B.S. degree in mechanical design and manufacturing and their automation and the M.S. degree in mechanical engineering from Harbin Institute of Technology, Harbin, China, in in 2018 and 2020, respectively. He is currently working toward the Ph.D. degree with the Department of Biomedical Engineering, National University of Singapore, Singapore

He was a Research Assistant with the Department of Mechanical and Energy Engineering, Southern University of Science and Technology, Shenzhen, China, from 2020 to 2021. His research interests including novel actuator, soft robotics and medical robotics.

**Xuanquan Liang** received the B.S. degree in physics in 2019 from Southern University of Science and Technology, Shenzhen, China, China, where he is currently working toward the Master degree with the Department of Mechanical and Energy Engineering.

His research interests including modern control method of electroadhesion systems, design and control of variable damper.

**Daiyue Wei** received the B.S. and M.S. degrees from the China University of Petroleum, Qingdao, China, and the South China University of Technology, Guangzhou, China, in 2017 and 2020, respectively. She is currently working toward with the Department of Medical Engineering, University of South Florida, Tampa, FL, USA

She was a Research Assistant with the Department of Mechanical and Energy Engineering, Southern University of Science and Technology, Shenzhen, China, from 2020 to 2022. Her research interests include two-dimensional materials and nanopore sequencing.

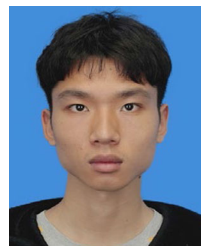

**Huacen Wang** received the B.S. degree in mechanical engineering in 2021 from Southern University of Science and Technology, Shenzhen, China, where he is currently working toward the M.S. degree with the Department of Mechanical and Energy Engineering.

His research interests including soft robotics and novel actuators.

**Renjie Zhu** (Graduate Student Member) received the B.S. degree in mechatronic engineering from Changchun University of Science and Technology, Changchun, China, in 2017, and the M.S. degree in biomedical engineering from Beihang University, Beijing, China, in 2020.

He is currently a Research Assistant with the Department of Mechanical and Energy Engineering, Southern University of Science and Technology. His research interests including miniature robotics and soft robotics.

**Ting Wang** received the B.S. degree in mechanical design and manufacturing and their automation from Southwest Jiaotong University, Chengdu, China, in 2013, and the M.S. degree in mechanical and electronical engineering from Huazhong University of Science and Technology, Wuhan, China, in 2016. She is currently working toward the Ph.D. degree with the Department of Biomedical Engineering, City University of Hong Kong, Hong Kong.

Her research interests including microrobotics, bionic robotics, advanced actuators, flapping-wing robots, micro aerial vehicles and medical robotics.

**Jianjun Mao** received the B.S. degree in mechanical design and manufacturing and their automation and the M.S. degree in mechanical engineering from Harbin Institute of Technology, Harbin, China, in 2018 and 2020, respectively.

He is currently a Mechanical Engineer with the Institute of Advanced Science Facilities, Shenzhen, China.

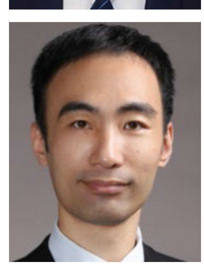

**Hongqiang Wang** (Member, IEEE) received the B.S. degree and M.S. degree in mechanical engineering from Xi’an Jiao Tong University, Xi’an, China, in 2008 and 2011, respectively, and the Ph.D. degree in precision mechanical engineering from Tokyo University, Tokyo, Japan, in 2015.

He is currently an Associate Professor with the Department of Mechanical and Energy Engineering, Southern University of Science and Technology, Chengdu, China. His research interests including miniature robotics, novel actuators, new flexible actuators, soft robotics and medical robotics.